arXiv:1002.1483v1 [cond-mat.str-el] 7 Feb 2010

Proposal to determine the Fermi-surface topology of a doped iron-based superconductor using bulk-sensitive Fourier-transform Compton scattering

Yung Jui Wang[1], Hsin Lin[1], B. Barbiellini[1], P.E. Mijnarends[1,2], S. Kaprzyk[1,3], R.S. Markiewicz[1] and A. Bansil[1]
[1] *Physics Department, Northeastern University, Boston, Massachusetts 02115, USA*
[2] *Department of Radiation, Radionuclides and Reactors, Faculty of Applied Sciences, Delft University of Technology, Delft, The Netherlands*
[3] *AGH University of Science and Technology, 30059 Krakow, Poland*

(Dated: February 7, 2010)

We have carried out first-principles calculations of the Compton scattering spectra to demonstrate that the filling of the hole Fermi surface in $LaO_{1-x}F_xFeAs$ produces a distinct signature in the Fourier transformed Compton spectrum when the momentum transfer vector lies along the [100] direction. We thus show how the critical concentration x_c, where hole Fermi surface pieces are filled up and the superconductivity mediated by antiferromagnetic spin fluctuations is expected to be suppressed, can be obtained in a bulk-sensitive manner.

PACS numbers: 71.18.+y, 71.20.-b, 74.25.Jb 74.70.Dd

The Fermi surface (FS) topology is a key ingredient for high temperature superconductivity in iron based layered pnictides. The so-called $s_\pm$ model[1–4] predicts superconducting gaps of one sign on the FS cylindrical hole sheets near $\Gamma(0,0)$ and of another sign on cylindrical electron sheets at $M(\pi,\pi)$. Doping x is needed to move the system away from the magnetic instabilities due to FS nesting[5–7]. In the superconducting material, spin fluctuations (related to residual FS nesting) may provide a glue for the Cooper pairs[1]. However, a complete filling of the hole FS at a certain electron doping will eventually lead to the suppression of the spin fluctuation glue. The exact value x_c of this critical doping might be affected by subtle correlations effects[8].

Experimental information regarding the FS topology comes mostly from angle resolved photoemission spectroscopy (ARPES) which is a surface sensitive probe.[5,9–12] . Moreover, since the doping level in the bulk could be different from that at the surface[2], the FS signal should be checked with bulk probes. Since the FS information from quantum oscillation studies[13,14] can be distorted because of the required high magnetic fields, we suggest determination of the FS topology via Compton scattering measurements.[15,16] In this letter, we show that a one dimensional Fourier transform of the Compton profile along [100] presents a large signal when the hole Fermi surface vanishes, providing a bulk sensitive method for determining the critical doping x_c for high temperature superconductivity in $LaO_{1-x}F_xFeAs$.

Recent advances in synchrotron light sources and detector technology have renewed interest in high-resolution Compton scattering as a bulk probe of fermiology related issues, see e.g., Refs.[17–20]. In a Compton scattering experiment, one measures a directional Compton profile (CP), $J(p_z)$, which is related to the twice integrated ground-state electron momentum density $\rho(p_x,p_y,p_z)$ by

$$J(p_z) = \int\int \rho(p_x,p_y,p_z)dp_x dp_y \ , \qquad (1)$$

for high momentum and energy transfer[21]. The exploration of FS topology with the aid of Compton scattering is complicated by the double integral in Eq. 1. As a result, FS breaks in $\rho(p_x,p_y,p_z)$ do not usually induce rapid variations in $J(p_z)$. A possible approach to deal with this problem is to measure CPs along many different directions and use state-of-the-art reconstruction methods based on the autocorrelation function $B(x,y,z)$ to obtain $\rho(p_x,p_y,p_z)$[22]. A much simpler and more robust method will be proposed in this letter.

The calculations presented here were performed within the local density approximation (LDA) using an all-electron fully charge self-consistent semi-relativistic Korringa-Kohn-Rostoker (KKR) method[23]. The compound $LaO_{1-x}F_xFeAs$ has a simple tetragonal structure (space-group P4/nmm). We have used the experimental lattice parameters[24] of $LaO_{0.87}F_{0.13}FeAs$ in which no spin-density-wave order was observed in neutron scattering experiments. Self-consistency was obtained for $x = 0$ and the effects of doping x were treated within a rigid band model by shifting the Fermi energy to accommodate the proper number of electrons[25–29]. The convergence of the crystal potential was approximately 10^{-4} Ry. The electron momentum density (EMD) $\rho(p_x,p_y,p_z)$ was computed on a fine mesh of 40.4×10^6 within a sphere of radius 12 a.u. in momentum space. To simulate the effect of resolution in high resolution Compton scattering experiments, the EMD has been been convoluted with a Gaussian characterized by a FWHM of 0.17 a.u.

Since the $LaO_{1-x}F_xFeAs$ electronic structure has a two-dimensional character, we shall focus on the calculated (001) 2D-projection of the momentum density given

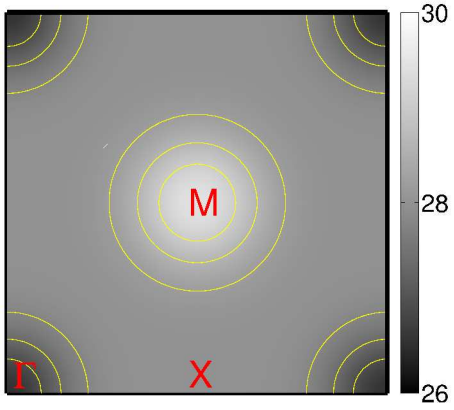

FIG. 1: (Color online) Calculated LCW distribution of in the paramagnetic tetragonal Brillouin zone of LaOFeAs.

by

$$\rho^{2D}(p_x, p_y) = \int \rho(p_x, p_y, p_z) dp_z \ . \tag{2}$$

In experiments, one adopts the so-called direct Fourier-transform method[22] to reconstruct $\rho^{2D}(p_x, p_y)$ from several directional CPs $J(p_z)$ measured in the (001) plane. This method uses the autocorrelation function $B(x, y, z)$ which is straightforwardly defined as the Fourier transformation of the momentum density

$$\begin{aligned} B(x, y, z) &= \int\int\int dp_x dp_y dp_z \\ &\times \ \rho(p_x, p_y, p_z) \exp[i(p_x x + p_y y + p_z z)] \ . \end{aligned} \tag{3}$$

Since $\rho(p_x, p_y, p_z)$ can be expressed as a sum over the momentum density of the natural orbitals $\psi_j(x, y, z)$[30] by using the convolution theorem, it can be shown that $B(x, y, z)$ is the autocorrelation of the natural orbitals

$$\begin{aligned} B(x, y, z) &= \sum_j n_j \int\int\int du dv dw \\ &\times \ \psi_j(x + u, y + v, z + w) \psi_j^*(u, v, w) \ , \end{aligned} \tag{4}$$

where n_j is the occupation number of the natural orbital $\psi_j(x, y, z)$. In the experiments $B(x, y, z)$ is obtained directly along a given direction by taking the 1D-Fourier transform of the CP along that direction. Then, once a set of B's has been calculated, a fine mesh is set up in real space and $B(x, y, z)$ is obtained at every mesh point by interpolation. Finally, if desired, an inverse Fourier transform of $B(x, y, 0)$ yields the distribution $\rho^{2D}(p_x, p_y)$. Our simulations reveal that the breaks in $\rho^{2D}(p_x, p_y)$ caused by FS crossings are scattered throughout momentum space with small weights given by matrix elements involving mostly the Fe d orbitals. Therefore, FS features are not easily detected directly in the $\rho^{2D}(p_x, p_y)$ distribution. However, as shown in Fig. 1 the Lock-Crisp-West (LCW) folding[31] can enhance FS breaks by coherently

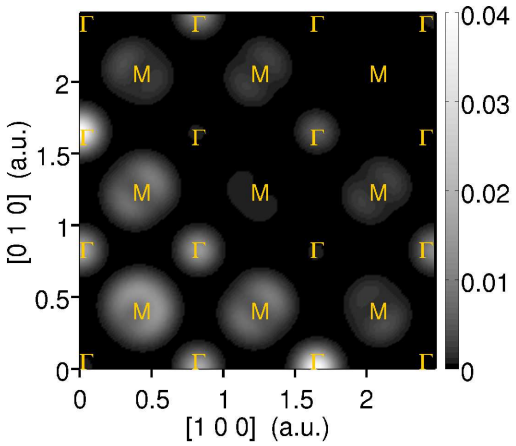

FIG. 2: (Color online) $\Delta\rho|_{x_1}^{x_2}(p_x, p_y)$ for $x_2 = 0.15$ and $x_1 = 0.10$. The yellow labels indicate the high symmetry positions Γ and M in momentum space.

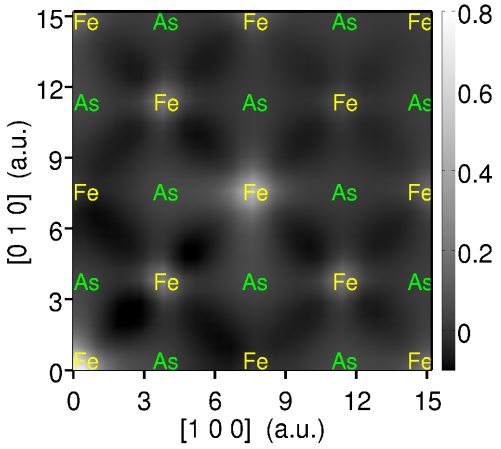

FIG. 3: (Color online) $\Delta B|_{x_1}^{x_2}(x, y)$ for $x_2 = 0.15$ and $x_1 = 0.10$. The yellow labels Fe indicate the atoms in the iron sublattice; green labels As indicate the (x, y)-projection of the atoms in the arsenic sublattice. Atomic assignments are based on assumption Fe is at origin.

superposing the umklapp terms according to

$$n(k_x, k_y) = \sum_{G_x, G_y} \rho^{2d}(k_x + G_x, k_y + G_y) \ , \tag{5}$$

where $n(k_x, k_y)$ gives the number of occupied states at the point (k_x, k_y) in the first Brillouin zone by summing over all projected reciprocal lattice vectors (G_x, G_y). The maximum of $n(k_x, k_y)$ at $M(\pi, \pi)$ is associated with the electron pockets while the minimum at Γ (0,0) is related to the hole pockets. Since the LCW folding can also enlarge artificial errors from the experimental data, below we will introduce a more robust means of extracting information about the evolution of the FS topology with doping.

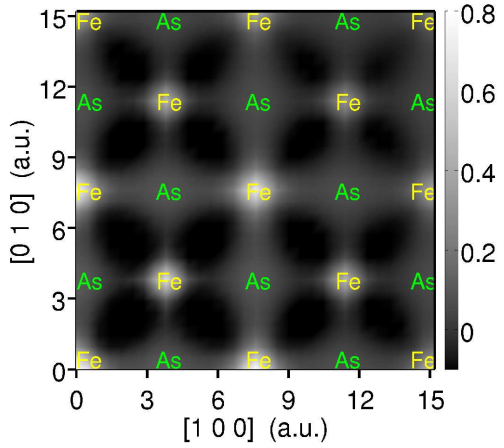

FIG. 4: (Color online) $\Delta B|_{x_1}^{x_2}(x,y)$. for $x_2 = 0.15$ and $x_1 = 0.10$, after artificially removing all the Bloch states around M. Atomic assignments are based on assumption Fe is at origin.

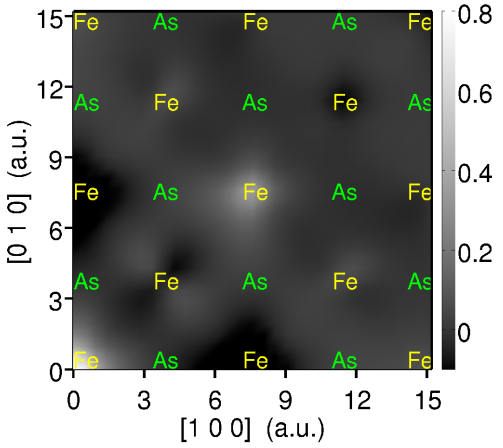

FIG. 5: (Color online) $\Delta B|_{x_1}^{x_2}(x,y)$. for $x_2 = 0.15$ and $x_1 = 0.10$, after artificially removing all the Bloch states around Γ. Atomic assignments are based on assumption Fe is at origin.

We can get more precise information on wave function symmetry near the Fermi surface (FS) by taking difference maps between two nearby dopings,

$$\Delta\rho|_{x_1}^{x_2}(p_x,p_y) = \rho^{2D}(p_x,p_y)|_{x_2} - \rho^{2D}(p_x,p_y)|_{x_1} \ , \quad (6)$$

where x_2 and x_1 are two different doping levels such that $x_2 > x_1$. The subtraction in Eq. 6 acts as a projector on the Fermi level subspace with the advantage of eliminating the large isotropic contribution of the core and some irrelevant valence electrons. The difference for $x_2 = 0.15$ and $x_1 = 0.10$ shown in Fig. 2 displays interesting FS effects strongly modulated by Fe d wave function effects. The corresponding Fourier transform $\Delta B|_{x_1}^{x_2}(x,y)$, Fig. 3, separates the different length scales in real space, which contribute to the oscillations in $\Delta\rho|_{x_1}^{x_2}(p_x,p_y)$. Thus, the peaks in the autocorrelation function ΔB indicate characteristic distances over which wave functions at the Fermi level are coherent. The peaks in Fig. 3 mostly stem from the Fe d orbitals since these largely dominate at the Fermi level[6]. In fact, from Fig. 3 one can see that the main peaks correlate very well with the iron sublattice. However, note that there are weaker features, marked "As", which correlate with the positions of the As atoms. Since the bands near the Fermi level mostly consist of Fe d_{xz}, d_{yz} and $d_{x^2-y^2}$ orbitals[32] , Fig. 3 reveals these characters in real space. To facilitate comparisons we normalize ΔB to unity at the origin.

We employ filtering techniques to enhance the sensitivity of the ΔB-maps to particular FS cylinders. Thus, in Fig. 4 we artificially remove the FS around M by applying a filter cutting out the Bloch states near M. As a result some Fe peaks essentially disappear, revealing the wavefunction characters of the Γ cylinders. In the same way, Fig. 5 shows the corresponding maps for the electron cylinders, generated by filtering out the cylinders at Γ . This filtering procedure can be tested by calculating $\Delta B|_{x_1}^{x_2}(x,y)$ at higher doping for x_2 and x_1, where the number of added electrons is sufficient to remove the hole cylinders at Γ without any filtering needed.[7,8,11,33] The result is very similar to Fig. 5, confirming that the present filter is an efficient way of sorting out contributions from different FS cylinders[34]. By comparing Fig. 4 and Fig. 5, it is clear that the hole FSs and the electron FSs give strikingly different contributions to $\Delta B|_{x_1}^{x_2}(x,y)$.

In Fig. 4 [hole FSs], there is a peak at every Fe site, with a corresponding weaker network of peaks at As sites. In contrast, for the electron contribution in Fig. 5, there are dips at some Fe sites and the As sites signatures are not visible. Some of these features can be readily understood with the phase factor $\exp(i\mathbf{k}\cdot\mathbf{r})$ of the Bloch wave function. At the band bottom, Γ, $\mathbf{k} = 0$ and all atoms are in phase (*bonding*). At the top of the band, (π,π), the phase factor is $(-1)^{m+n}$ – i.e., perfectly *antibonding*. Since the FSs are small cylinders near Γ and (π,π) respectively, their ΔB-maps are dominated by this interference term.

Interestingly, in Fig. 6, we show[35] the contrasting behavior of the autocorrelation function ΔB near the second neighbor Fe, at a distance about 7.6 a.u. from the origin along the [100]-direction. The minimum is produced by anti-bonding states belonging to the M FSs while the maximum is the result of bonding states belonging to the Γ FSs. Hence with doping the feature should evolve from the red curve when both FS are occupied to the green curve when the Γ FS disappears.

Since this last analysis will need only one FT of the experimental Compton profile along [100] it clearly provides particularly robust FS information in real space. In contrast, the ρ^{2D} reconstruction requires many more numerical manipulations[22] and therefore it can be less reliable. Our ΔB methodology thus is a more reliable way to detect when the FS signal at Γ vanishes.

In conclusion, our study predicts that high-resolution

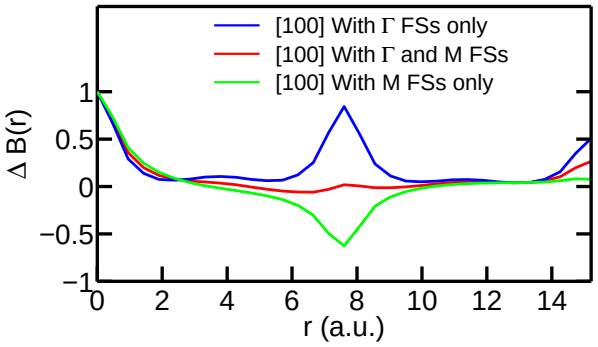

FIG. 6: (Color online) Cut of ΔB along the [100] direction.

Compton scattering spectra will yield signatures for the FS topology of Fe-based superconductors. In particular, the ΔB-map projected along the [100] direction displays a remarkable signature of the FS evolution with doping. Thus our method gives a robust way to establish the topology rather than the precise shape of the iron pnictides FS. These results indicate that Compton scattering can provide a powerful new spectroscopic window for investigating FSs compatible with the $s_{\pm}$ model for the description of the superconducting order parameter in the Fe-based superconductors.

We are grateful to M. Lindroos, Y. Sakurai, Z. Hasan and T. Jarlborg for important discussions. This work is supported by the US Department of Energy, Office of Science, Basic Energy Sciences contract DE-FG02-07ER46352, and benefited from the allocation of supercomputer time at NERSC and Northeastern University's Advanced Scientific Computation Center (ASCC). It was also sponsored by the Stichting Nationale Computer Faciliteiten (NCF) for the use of supercomputer facilities, with financial support from NWO (Netherlands Organization for Scientific Research).

[1] I. I. Mazin *et al.*, Phys. Rev. Lett. **101**, 057003 (2008).
[2] I. I. Mazin and J. Schmalian, Physica C **469**, 614 (2009).
[3] A. V. Chubukov, D. V. Efremov, and I. Eremin, Phys. Rev. B **78**, 134512 (2008).
[4] A. V. Chubukov, I. Eremin and M. M. Korshunov, Phys. Rev. B **79**, 220501(R) (2009).
[5] M. R. Norman, Physics **1**, 21 (2008).
[6] D. J. Singh and M.-H. Du, Phys. Rev. Lett. **100**, 237003 (2008).
[7] I. I. Mazin *et al.*, Phys. Rev. B **78**, 085104 (2008).
[8] K. Haule, J. H. Shim, and G. Kotliar, Phys. Rev. Lett. **100**, 226402 (2008).
[9] K. Terashima *et al.*, Proc. Nat. Acad. Sci. **106**, 7330 (2009).
[10] D. H. Lu *et al.*, Physica C **469**, 452 (2009).
[11] Y. Sekiba *et al.*, New J. Phys. **11**, 025020 (2009).
[12] S. Sahrakorpi *et al.*, Phys. Rev. Lett. **95**, 157601 (2005).
[13] A. I. Coldea *et al.*, Phys. Rev. Lett. **101**, 216402 (2008).
[14] J. G. Analytis *et al.*, Phys. Rev. Lett. **103**, 076401 (2009).
[15] Positron annihilation would provide another bulk-sensitive probe of the Fermi surface. See, e.g., Ref. 16.
[16] L. C. Smedskjaer *et al.*, J. Phys. Chem. Solids **52**, 1541 (1991); P. E. Mijnarends *et al.*, J. Physics: Conden. Matter 10, 10383 (1998).
[17] Y. Tanaka *et al.*, Phys. Rev. B **63**, 045120 (2001).
[18] S. Huotari *et al.*, Phys. Rev. B **62**, 7956 (2000).
[19] G. Stutz *et al.*, Phys. Rev. B **60**, 7099 (1999).
[20] M.J. Cooper *et al.* (editors), *X-Ray Compton Scattering*, Oxford University Press, Oxford (2004).
[21] I. G. Kaplan, B. Barbiellini and A. Bansil, Phys. Rev. B **68**, 235104 (2003).
[22] I. Matsumoto *et al.*, Phys. Rev. B **64**, 045121 (2001).
[23] A. Bansil *et al.*, Phys. Rev. B **60**, 13396 (1999).
[24] Y. Qiu *et al.*, Phys. Rev. B **78**, 052508 (2008).
[25] A more sophisticated treatment using KKR-CPA or other approaches [see, e.g., Refs. 26-29] was not undertaken.
[26] A. Bansil, Zeitschrift Naturforschung A **48**, 165 (1993); A. Bansil, Phys. Rev. B20, 4035 (1979).
[27] L. Schwartz and A. Bansil, Phys. Rev. B **10**, 3261 (1974).
[28] S. N. Khanna *et al.*, Solid State Commun. **55**, 223 (1985).
[29] H. Lin *et al.*, Phys. Rev. Lett. **96**, 097001 (2006).
[30] B. Barbiellini, A. Bansil, J. Phys. Chem. Solids **62**, 2181 (2001).
[31] D.G. Lock, V.H.C. Crisp, and R.N. West, J. Phys. F: Met. Phys. **3**, 561 (1973).
[32] C.-C. Lee, W.-G. Yin and W. Ku, Phys. Rev. Lett. **103**, 267001 (2009).
[33] The exact value of x_2 is sensitive to the assumption of rigid band filling and to the exchange-correlation functional used (See Refs. 7 and 8).
[34] This filtering procedure can also be applied to experimental Compton data.
[35] The cut of ΔB with Γ FS is derived from $\Delta B|_{x_1}^{x_2}(x,y)$ for $x_2 = 0.15$ and $x_1 = 0.10$, while the cut of ΔB without Γ FS is obtained from $\Delta B|_{x_1}^{x_2}(x,y)$ for $x_2 = 0.15$ and $x_1 = 0.10$, after artificially removing all the Bloch states around Γ.